

Investigations on 10-Hz sub-Joule fs-laser pumped neon- and nickel-like X-ray lasers

R. Tommasini, J. Nilsen, E. E. Fill

This article was submitted to
2001 International Symposium on Optical Science and Technology
San Diego, CA
July 29 through August 3, 2001

U.S. Department of Energy

Lawrence
Livermore
National
Laboratory

August 13, 2001

DISCLAIMER

This document was prepared as an account of work sponsored by an agency of the United States Government. Neither the United States Government nor the University of California nor any of their employees, makes any warranty, express or implied, or assumes any legal liability or responsibility for the accuracy, completeness, or usefulness of any information, apparatus, product, or process disclosed, or represents that its use would not infringe privately owned rights. Reference herein to any specific commercial product, process, or service by trade name, trademark, manufacturer, or otherwise, does not necessarily constitute or imply its endorsement, recommendation, or favoring by the United States Government or the University of California. The views and opinions of authors expressed herein do not necessarily state or reflect those of the United States Government or the University of California, and shall not be used for advertising or product endorsement purposes.

This is a preprint of a paper intended for publication in a journal or proceedings. Since changes may be made before publication, this preprint is made available with the understanding that it will not be cited or reproduced without the permission of the author.

This report has been reproduced
directly from the best available copy.

Available to DOE and DOE contractors from the
Office of Scientific and Technical Information
P.O. Box 62, Oak Ridge, TN 37831
Prices available from (423) 576-8401
<http://apollo.osti.gov/bridge/>

Available to the public from the
National Technical Information Service
U.S. Department of Commerce
5285 Port Royal Rd.,
Springfield, VA 22161
<http://www.ntis.gov/>

OR

Lawrence Livermore National Laboratory
Technical Information Department's Digital Library
<http://www.llnl.gov/tid/Library.html>

Investigations on 10-Hz sub-Joule fs-laser pumped neon- and nickel-like X-ray lasers

Riccardo Tommasini,^a Joseph Nilsen^b and Ernst E. Fill^a

^aMax-Planck-Institut fuer Quantenoptik D-85748 Garching, Germany

^bLawrence Livermore National Laboratory Livermore, California 94550, USA

ABSTRACT

Experimental investigations on the conditions to achieve transient gain in neon-like Ti and nickel-like molybdenum XUV laser pumped by a 10-Hz sub-Joule femtosecond laser are presented. The 4d-4p ($J=0-1$) $\lambda=18.9$ nm and 4f-4d ($J=1-1$) $\lambda=22.6$ nm lines in Ni-like Mo as well as the 3p-3s ($J=0-1$) $\lambda=32.6$ nm line in neon-like titanium have been observed. The Ni-like laser lines show a threshold behavior with respect to the pump irradiance as they appear only above 10^{15} W/cm². Simulation for the fs-laser pumped Ni-like Mo XUV laser are also presented.

Keywords: x-ray lasers, transient gain, collisional excitation, traveling wave excitation

1. INTRODUCTION

Due to the use of the prepulse technique,¹ neon-like and nickel-like soft-X-ray lasers are routinely realized using electron collisional excitation. Much progress has been made in reducing the size of the pump laser from the large ICF (Inertial Confinement Fusion) lasers²⁻⁴ using long pulses ($\gtrsim 100$ ps) to the ps pulse CPA (Chirped Pulse Amplification) systems⁵⁻⁷ with energies down to 5 J. However the major limitations of these devices are still the size, the costs, and the low repetition rates (time delay between shots $\gtrsim 4$ minutes) that are dictated by the cooling times of the amplifier stages of the driving lasers.

Practical applications of such laser sources as a scientific tool requires more compact dimensions and higher repetition rates.

We present experiments that demonstrate the feasibility of both Ne-like and Ni-like X-ray lasers driven by a high-repetition (10 Hz), low-energy (300 mJ) pump laser used in a traveling wave configuration.

2. EXPERIMENTAL SETUP

The experiments were carried out by means of the setup shown in Fig.1. Pulses from the ATLAS titanium-sapphire laser, delivering an energy of 300 mJ in 150 fs, at a central wavelength of 790 nm, are focused onto target by a gold-coated cylindrical mirror in oblique incidence configuration. The 60 degrees of incidence angle produce a velocity of excitation along the 50- μ m-wide line-focus equal to $1.15 c$, c being the velocity of light. A cylindrical lens placed before the cylindrical mirror and with axis orthogonal to the mirror axis is used to adjust the length of the line-focus between 3 mm and 6 mm, thus producing an irradiance on target between $6 \cdot 10^{14}$ W/cm² and $1.2 \cdot 10^{15}$ W/cm². A 2% prepulse is produced by an optical delay line consisting of four mirrors in a dog-leg arrangement. The mainpulse-prepulse delay time is 1.3 ns. The targets are flat slabs of Mo or Ti and the diagnostics consist of a 0.8 μ m Al filter, a (5000 lines/mm) transmission grating and a CCD camera.

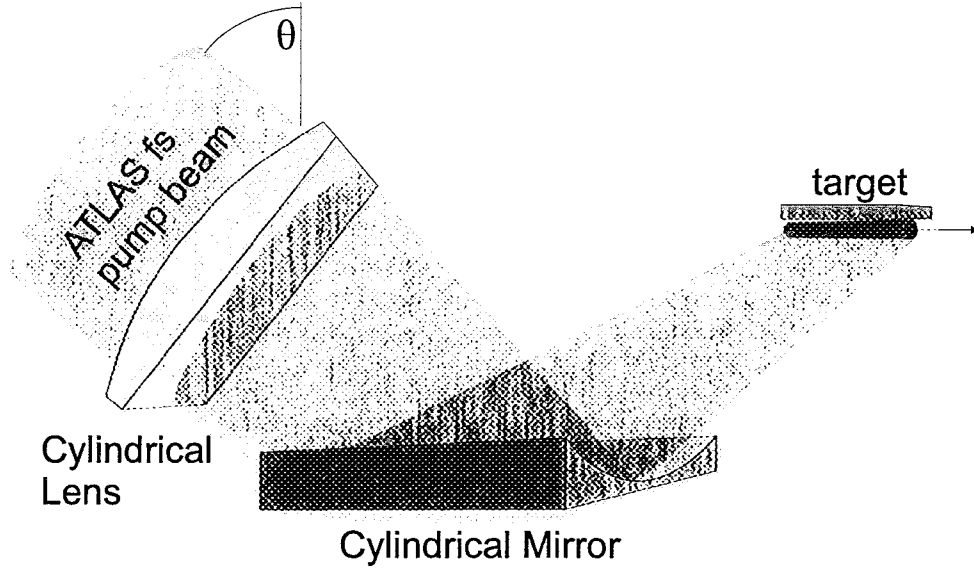


Figure 1. Experimental setup. The 10-Hz Ti:Sa ATLAS laser delivers 300 mJ/150 fs @ 790 nm with a 2% prepulse and a mainpulse–prepulse delay fixed at 1.3 ns. The 50- μ m-wide line-focus can be adjusted between 3 and 6 mm by changing the distance of the cylindrical lens from the cylindrical mirror, giving an irradiance on target: $\approx 6 \cdot 10^{14}$ – $1.2 \cdot 10^{15}$ W/cm². Due to 60° oblique incidence on target, TWE is achieved with $v_{ex} = 1.15$ c.

3. EXPERIMENTAL RESULTS

Figure 2 shows the axial spectrum of Mo for a 6-mm long line-focus, i.e. $6 \cdot 10^{14}$ W/cm² as an irradiance on target. The Al L edge is clearly visible together with some Oxygen lines (O^{5+} and O^{4+}) due to impurities into the vacuum chamber. No other lines are clearly distinguishable. An "a-posteriori" comparison with Fig.3 helps us to identify weak lines from Cu-like Mo at 18.3 nm ($5p_{3/2}$ – $4d_{5/2}$) and 18.6 nm ($5p_{1/2}$ – $4d_{3/2}$) and a barely visible laser line from Ni-like Mo at 18.9 nm ($4d$ – $4p$, $J=0-1$).

Figure 3 shows the axial spectrum of Mo for a 3-mm long line-focus, i.e. $1.2 \cdot 10^{15}$ W/cm² as an irradiance on target. While the lines from Cu-like Mo are more contrasted, the difference with the spectrum at lower irradiance is the clear build-up of the Ni-like Mo lines: the $4d$ – $4p$ ($J=0-1$), $\lambda=18.9$ nm line, predicted to have the largest gain and the $4f$ – $4d$ ($J=1-1$), $\lambda=22.6$ nm self-photopumped line.⁸ The observation of the Ni-like Mo laser lines is erratic and the two lines do not always appear together in the spectrum. This confirms a threshold-like behavior with respect to the pump energy and the fact that our operating conditions are very near to threshold.

Figure 4 shows the axial spectrum of Ti for a 3-mm long line-focus and hence $1.2 \cdot 10^{15}$ W/cm² as an irradiance on target. The $3p$ – $3s$ ($J=0-1$), $\lambda=32.6$ nm line from Ne-like Ti is evident.

As a general comment to these results we can say that, due to the small amount of pump energy, much smaller regions of hot plasma are achievable with respect to high-power pump lasers. In any case the major problem seems to be the short and weak prepulse which makes it difficult to meet the proper conditions for lasing: a too short main–pre-pulse delay, to exploit hot pre-plasma conditions, leads to high electron density gradients and hence to refraction losses, while a longer delay, aimed to find a smooth electron density distribution, leads to a too cold pre-plasma. A longer, on the scale of ns, and more energetic prepulse should solve the situation. This

Further author information: (Send correspondence to R. Tommasini)
R. Tommasini: Email: r.tommasini@mpq.mpg.de, Telephone: +49 89 32905728

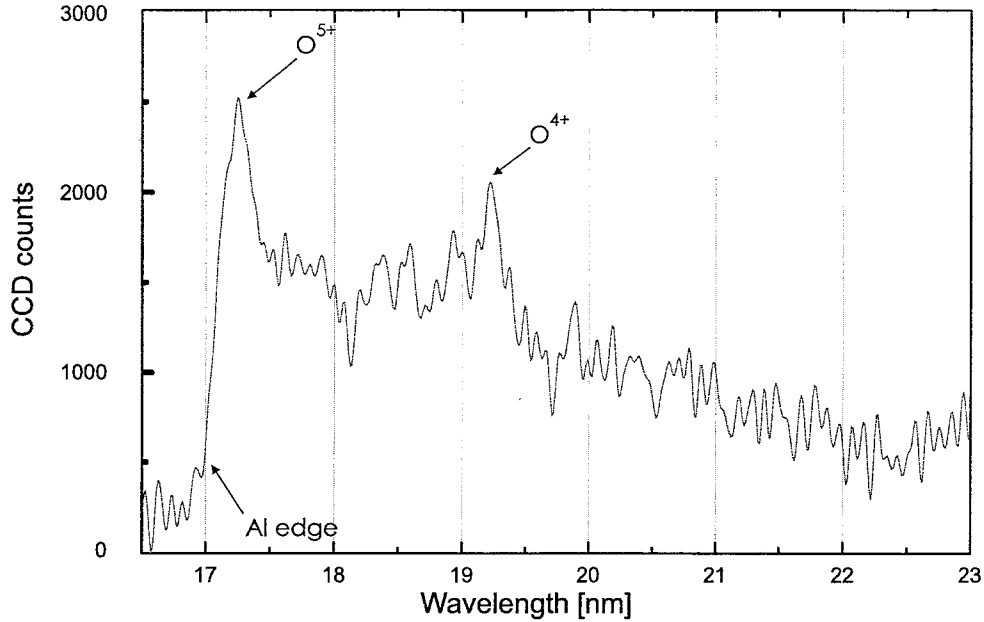


Figure 2. Mo axial spectrum for a 6-mm long line-focus and $6 \cdot 10^{14}$ W/cm² irradiance on target. Mo lines are not clearly distinguishable. Oxygen lines originate from impurities.

is confirmed by the results from simulations to be discussed later on. Nonetheless the observation of emission on the lasing lines of Ne-like Ti and Ni-like Mo gives indications of possible population inversion, while the results shown from Ni-like Mo give evidence of near-threshold conditions with respect to pump energy.

4. SIMULATIONS

To model the Mo experiments we did LASNEX one-dimensional (1D) computer simulations of a Mo slab illuminated under conditions similar to the experimental conditions. The LASNEX calculations were 1D calculations but include an expansion angle of 15 degrees in the dimension perpendicular to the primary expansion so as to simulate 2D effects.

The LASNEX calculated densities and temperatures are used as input to the CRETIN code,⁹ which calculates the gains of the laser lines including radiation trapping effects for the four strong 4f and 4p \rightarrow 3d resonance lines in Ni-like Mo. Bulk Doppler effects due to the expansion of the plasmas were also included. The Mo atomic model used by the CRETIN code includes all 107 detailed levels for levels up to $n = 4$ in Ni-like Mo.

Two dominant laser lines are predicted; the 4d $^1S_0 \rightarrow$ 4p 1P_1 line at 18.9 nm and the 4f $^1P_1 \rightarrow$ 4d 1P_1 line at 22.6 nm. The Ni-like 4d $^1S_0 \rightarrow$ 4p 1P_1 line lases by having monopole collisional excitation from the ground state populate the upper laser level. The lower laser level is depopulated by fast radiative decay to the ground state. In contrast, the 4f $^1P_1 \rightarrow$ 4d 1P_1 line lases because radiation trapping allows a large radiation field to build up on the 3d $^1S_0 \rightarrow$ 4f 1P_1 resonance line and populate the 4f upper laser state by the self-photopumping process.⁸ For convenience we leave out the 3d 9 electrons which are common to both states.

Figure 5 shows the gain versus space and time for the 4d $^1S_0 \rightarrow$ 4p 1P_1 laser line at 18.9 nm and the 4f $^1P_1 \rightarrow$ 4d 1P_1 line at 22.6 nm. The mainpulse peaks at 1 ps on this time scale. The horizontal axis gives the distance from the target surface in the direction of the plasma expansion. The gray scale varies from 0 to

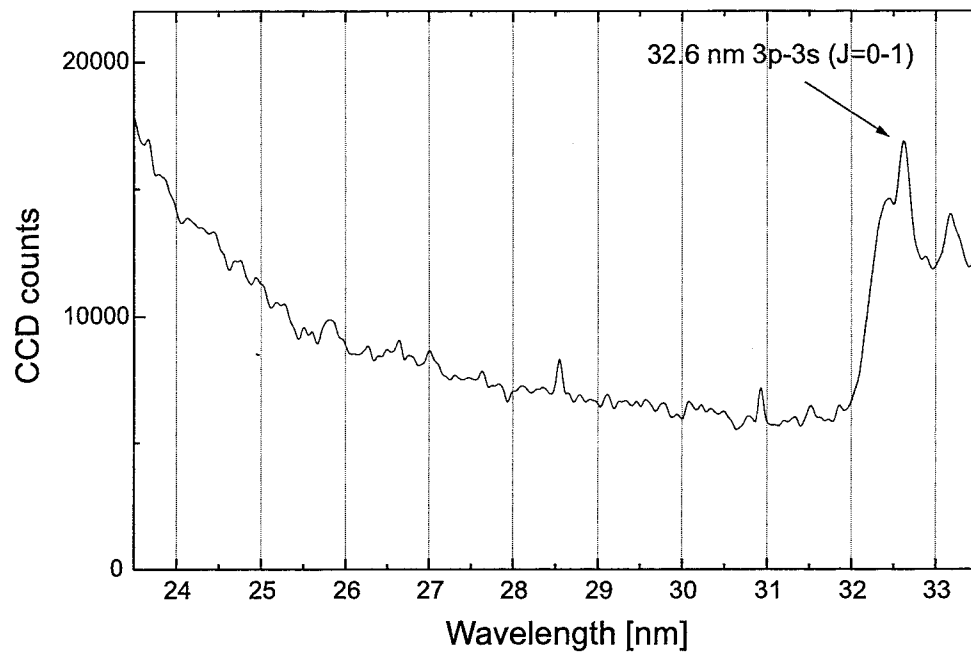


Figure 4. Ti axial spectrum for a 3-mm long line-focus and $1.2 \cdot 10^{15} \text{ W/cm}^2$ irradiance on target. The 3p-3s ($J=0-1$), $\lambda=32.6 \text{ nm}$ line from Ne-like Ti is evident.

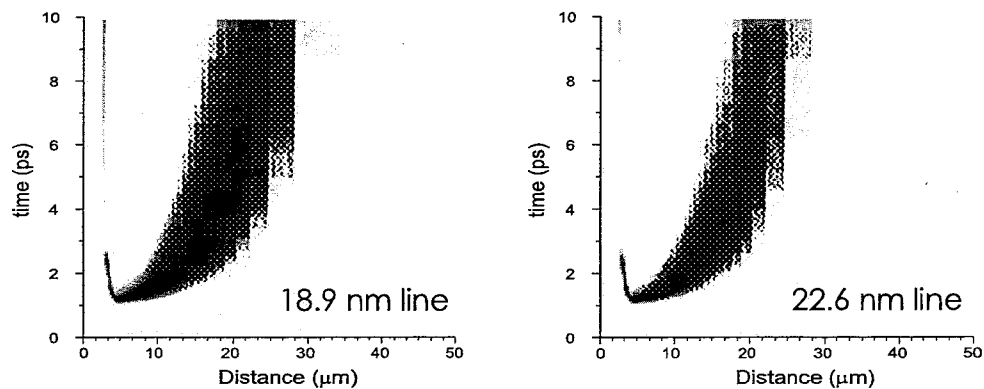


Figure 5. Gain contours vs. space and time for the 18.9-nm and 22.6-nm laser line of Ni-like Mo as calculated by the CRETIN code with hydrodynamic simulations from LASNEX as input. The main pulse peaks at 1 ps on this time scale.

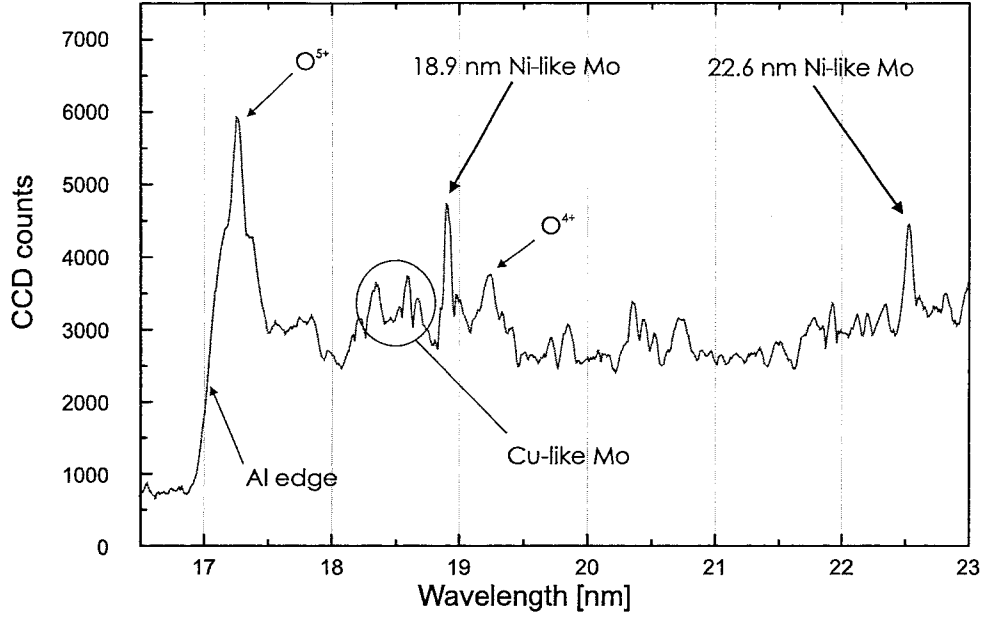


Figure 3. Mo axial spectrum for a 3-mm long line-focus and $1.2 \cdot 10^{15} \text{ W/cm}^2$ irradiance on target. Ni-like Mo lines appear: the 4d-4p ($J=0-1$), $\lambda = 18.9 \text{ nm}$ line, predicted to have the largest gain and the 4f-4d ($J=1-1$), $\lambda = 22.6 \text{ nm}$ self-photopumped line. Cu-like Mo lines are also seen, but at lower intensity.

300 cm^{-1} with the darkest region representing gains greater than 300 cm^{-1} . Peak values for the gain are nearly the same for the two lines but the 18.9 nm line shows a larger gain region in both space and time.

The peak temperature exceeds 1 keV at a distance of $4.5 \mu\text{m}$ at 1.1 ps but most of the plasma with high gain has temperatures below 500 eV. In Fig.6 we plot the electron temperature versus time at a position $14 \mu\text{m}$ from the target surface. One observed that the temperature quickly reaches a peak of 370 eV and then slowly cools down. The excitation energy for the 18.9 nm line is 316 eV. As long as the temperature stays above 180 eV we still have 50% of the maximum excitation rate which occurs at twice the excitation energy.

If we look at a time of 2 ps where the gain is very strong one predicts peak gain of 342 cm^{-1} for the 18.9 nm line at $11.6 \mu\text{m}$ from the surface where the electron temperature is 392 eV, the ion temperature is 3.5 eV, and the electron density is $3.6 \cdot 10^{20} \text{ cm}^{-3}$. The FWHM spatial extent of the gain is only $5 \mu\text{m}$. If we now look at one spatial point about $14 \mu\text{m}$ from the surface the FWHM temporal extent of the gain lasts for only 2 ps. For the 22.6 nm line the temporal and spatial extent of the gain is even smaller. Hence both lines show an extremely small gain region. The weak 150 fs prepulse (2%) creates a relatively cold plasma. The main pulse then needs to do all the heating and ionization of the plasma. A longer, larger prepulse would couple better and create a larger, more ionized plasma. Calculations done using a 60 mJ, 500 ps prepulse show a larger plasma and gain region for both lines.

5. REFRACTION LOSSES AND EFFICIENT TWE

Severe limitations to fully exploit the gain arise from refraction due to the steep electron density ∇n_e gradient and from the temporal mismatch between the velocity of the excitation and the group velocity of the amplified pulse along the gain medium,^{10,11} i.e. a mismatched TWE. We can evaluate both effects by taking into account the simulation results for the electron density and gain. We take as a reference the conditions at 2 ps, indicating a

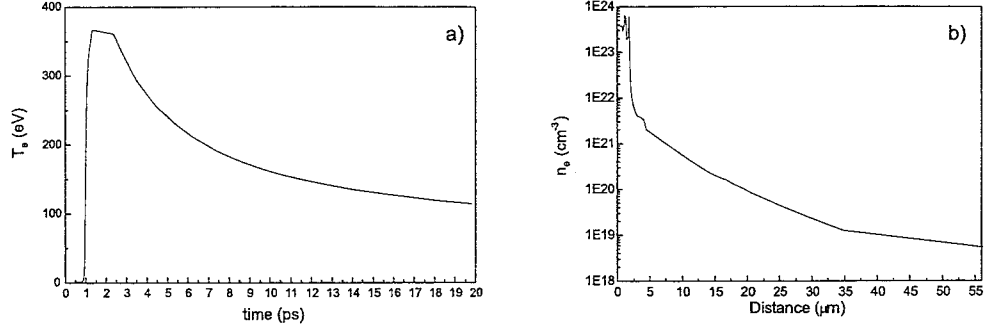


Figure 6. a): Electron temperature versus time at a position $14 \mu\text{m}$ from the target surface as calculated by the LASNEX code. The mainpulse peaks at 1 ps on this time scale. b): Electron density versus distance from target at a time of 2 ps as calculated by the LASNEX code.

gain of 342 cm^{-1} and 272 cm^{-1} , at about $11.5 \mu\text{m}$ from the target surface, for the 18.9 nm line and the 22.6 nm lines, respectively (see Fig.5). The corresponding values for the FWHM of the gain are $5 \mu\text{m}$ and $4 \mu\text{m}$. The electron density is $3.6 \cdot 10^{20} \text{ cm}^{-3}$ with a gradient equal to $-7.7 \cdot 10^{23} \text{ cm}^{-4}$ (see Fig.6).

Given these values, we calculate the distance l_r along the propagation direction at which a ray bends out from the gain region^{12,13}: $l_r = 0.9 \text{ mm}$ and $l_r = 0.8 \text{ mm}$ for the 18.9 nm and 22.6 nm lines, respectively. These deviations can be compensated using bent targets with a curvature radius of $\approx 8 \text{ cm}$, or a longer prepulse.

To estimate the effect of the temporal mismatch arising from a non perfect TWE, we take the gain peak values given above and the gain lifetimes of 2 ps and 1 ps, as they result from simulations for the 18.9 nm line and 22.6 nm line respectively. Assuming traveling wave excitation at the speed of light, we can thus calculate the distance l_{TW} along which the amplified pulse is still within the gain lifetime.¹⁰ It results that the soft-X-ray photons experience gain on distances of only $l_{TW} = 0.8 \text{ mm}$ for the 18.9 nm line and $l_{TW} = 0.4 \text{ mm}$ for the 22.6 nm line. Traveling wave excitation at velocities below the speed of light can be used to overcome this last limitation.¹¹

A pump geometry which may solve both problems simultaneously is shown in Fig.7, where a step mirror placed on the optical path of the short fs mainpulse is used together with oblique incidence to achieve sub-c TWE, while the longer prepulse is provided by a synchronized ns laser.

6. CONCLUSIONS

Using a sub-Joule 10-Hz fs laser as a pump, the 4d-4p ($J=0-1$) $\lambda = 18.9 \text{ nm}$ and 4f-4d ($J=1-1$) $\lambda = 22.6 \text{ nm}$ lines in Ni-like Mo as well as the 3p-3s ($J=0-1$) $\lambda = 32.6 \text{ nm}$ line in Ne-like Ti have been observed. By changing the line-focus length of the pump laser, we observed that Ni-like laser lines in Mo appear only above 10^{15} W/cm^2 . These results demonstrate the feasibility of using high-repetition-rate, sub-Joule pump lasers in realizing X-ray lasers from collisional-excitation laser-produced plasmas. A prepulse on the ns scale is required to provide a more extended gain medium. Finally we notice that further improvement in the performance is expected using sub-c TWE.

ACKNOWLEDGMENTS

The authors thank Prof. K. Witte for continuous encouragement, the ATLAS facility crew for the experimental support, and Mr. W. Fölsner for help in target preparation.

This work was supported by the European TMR Programme, under contract number ERBFMRXCT98-0185, and by the Commission of the European Communities within the framework of the Euratom Max-Planck-Institut für Plasmaphysik Association.

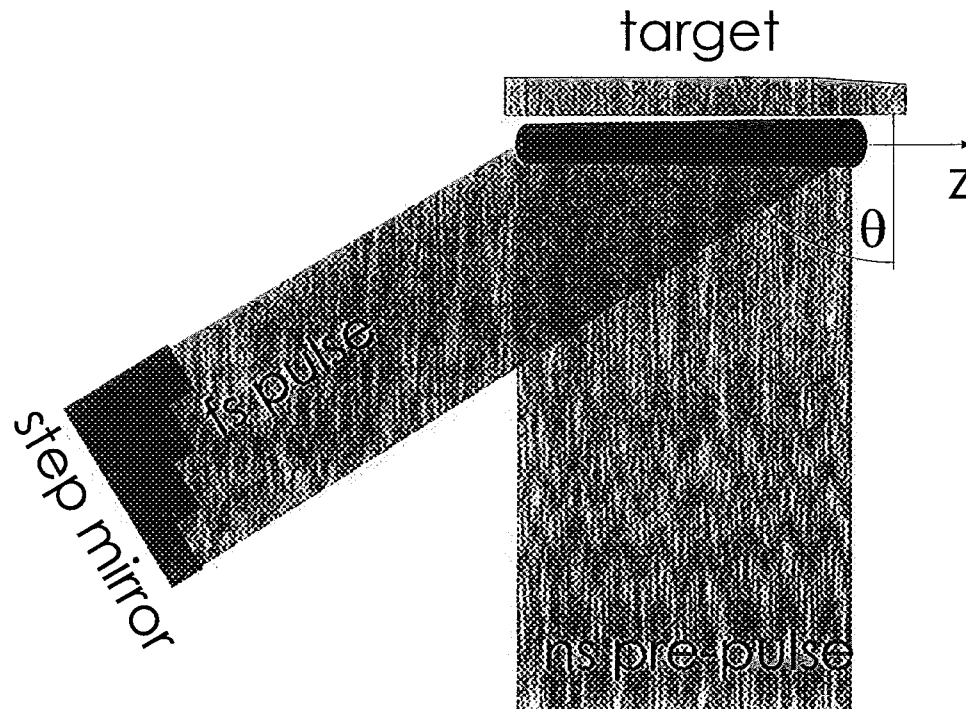


Figure 7. Step-mirror and oblique incidence to realize sub-c TWE from a fs laser. Prepulse is provided by a synchronized ns laser.

The work of one of the authors (J.N.) was performed under the auspices of the U. S. Department of Energy by the University of California Lawrence Livermore National Laboratory under contract No.W-7405-ENG-48.

REFERENCES

1. J. Nilsen, B. J. MacGowan, L. B. Da Silva, and J. C. Moreno, "Prepulse technique for producing low-z ne-like x-ray lasers," *Physical Review A* **48**(6), pp. 4682-5, 1993.
2. H. Daido, Y. Kato, K. Murai, S. Ninomiya, R. Kodama, G. Yuan, Y. Oshikane, M. Takagi, H. Takabe, and F. Koike, "Efficient soft x-ray lasing at 6 to 8 nm with nickel-like lanthanide ions," *Physical Review Letters* **75**(6), pp. 1074-7, 1995.
3. E. E. Fill, Y. L. Li, D. Schlogl, J. Steingruber, and J. Nilsen, "Sensitivity of lasing in neonlike zinc at 21.2 nm to the use of the prepulse technique," *Optics Letters* **20**(4), pp. 374-376, 1995.
4. J. Nilsen and J. C. Moreno, "Lasing at 7.9 nm in nickellike neodymium," *Optics Letters* **20**(12), pp. 1386-8, 1995.
5. P. V. Nickles, V. N. Shlyaptsev, M. Kalachnikov, M. Schnurer, I. Will, and W. Sandner, "Short pulse x-ray laser 32.6 nm based on transient gain in ne-like titanium," *Physical Review Letters* **78**(14), pp. 2748-2751, 1997.
6. J. Dunn, A. L. Osterheld, R. Shepherd, W. E. White, V. N. Shlyaptsev, and R. E. Stewart, "Demonstration of x-ray amplification in transient gain nickel-like palladium scheme," *Physical Review Letters* **80**(13), pp. 2825-2828, 1998.

7. J. Dunn, J. Nilsen, A. L. Osterheld, Y. Li, and V. N. Shlyaptsev, "Demonstration of transient gain x-ray lasers near 20 nm for nickellike yttrium, zirconium, niobium, and molybdenum," *Optics Letters* **24**(2), pp. 101–3, 1999.
8. J. Nilsen, "Design of a picosecond-laser-driven ni-like mo x-ray laser near 20 nm," *Journal of the Optical Society of America B* **14**(6), pp. 1511–1514, 1997.
9. H. A. Scott, "Cretin - a radiative transfer capability for laboratory plasmas," *JQSRT* **71**(689-701), 2001.
10. R. Tommasini and E. Fill, "Excitation velocity and group velocity mismatch in amplified spontaneous emission lasers: A discussion on the transient gain x-ray lasers," *Physical Review A* **62**, p. 034701, 2000.
11. R. Tommasini and E. Fill, "Effective traveling wave excitation below the light speed," *Optics Letters* **26**(10), pp. 689 – 691, 2001.
12. J. G. Lunney, "Waveguiding in soft x-ray laser experiments," *Applied Physics Letters* **48**(14), pp. 891–3, 1986.
13. E. E. Fill, "Ray trajectories in line-focused laser plasmas," *Journal of the Optical Society of America B* **14**(6), pp. 1505–1510, 1997.

University of California
Lawrence Livermore National Laboratory
Technical Information Department
Livermore, CA 94551

1. The first part of the document is a title page. It contains the title of the document, the author's name, and the date of the document.

2. The second part of the document is an abstract. It provides a brief summary of the main points of the document.

3. The third part of the document is an introduction. It provides background information on the topic and states the purpose of the document.

4. The fourth part of the document is the main body. It contains the main text of the document, which is divided into several sections.

5. The fifth part of the document is a conclusion. It summarizes the main findings of the document and provides a final statement.

6. The sixth part of the document is a bibliography. It lists the sources of information used in the document.

7. The seventh part of the document is an appendix. It contains additional information that is related to the main text but is not essential for understanding the main points.

8. The eighth part of the document is a glossary. It defines the key terms used in the document.

9. The ninth part of the document is an index. It provides a list of the main topics and sub-topics covered in the document.

10. The tenth part of the document is a list of figures and tables. It provides a list of the visual elements included in the document.